Society of Medical Education & Research

2026, Volume 6, Issue 1, Page No: 39-59
ISSN: 3108-4834

Archive of International Journal of Cancer and Allied Science

S-Palmitoylation of FASN by ZDHHC20 Promotes Hepatocellular Carcinogenesis by Preventing Ubiquitin-Mediated Degradation

Nora Schneider[1]*, Tobias Frank[1], Andreas Müller[2], Christoph Meier[3]

[1]Department of HCC Biology and Protein Palmitoylation, Faculty of Medicine, University of Freiburg, Freiburg, Germany.
[2]Department of Fatty Acid Synthase and Oncogenesis, Faculty of Medicine, Heidelberg University, Heidelberg, Germany.
[3]Department of Protein Degradation and Ubiquitination, Faculty of Medicine, University of Hohenheim, Stuttgart, Germany.

***E-mail** ✉ nora.schneider@natfak.uni-freiburg.de

Abstract

Protein palmitoylation is a reversible lipid modification that plays pivotal roles in various physiological processes. Aberrant palmitoylation frequently contributes to cancer development. However, the precise contributions of S-palmitoylating enzymes, known as palmitoyltransferases, to the initiation and progression of hepatocellular carcinoma (HCC) remain poorly understood. The role of zinc finger DHHC-type palmitoyltransferase 20 (ZDHHC20) in HCC tumorigenesis was assessed using diethylnitrosamine (DEN)-induced and DEN plus CCl4 HCC mouse models in ZDHHC20 knockout animals. To delineate the downstream targets and molecular mechanisms of ZDHHC20, the study employed palmitoylation liquid chromatography-mass spectrometry analysis, acyl-biotin exchange assay, co-immunoprecipitation, ubiquitination assays, protein half-life assays, and immunofluorescence microscopy. Genetic ablation of ZDHHC20 markedly suppressed hepatocarcinogenesis triggered by chemical carcinogens in both in vivo HCC mouse models. Palmitoylation profiling identified 97 proteins harboring 123 cysteine residues that undergo ZDHHC20-dependent palmitoylation. Notably, fatty acid synthase (FASN) was palmitoylated by ZDHHC20 at cysteine sites 1471 and 1881. Either genetic deletion or pharmacological blockade of ZDHHC20, along with substitution mutations at the critical FASN cysteines (C1471S/C1881S), accelerated FASN degradation. ZDHHC20-catalyzed palmitoylation of FASN further antagonized its breakdown via the ubiquitin-proteasome system mediated by the E3 ubiquitin ligase complex SNX8-TRIM28. The results underscore the essential function of ZDHHC20 in driving hepatocarcinogenesis and uncover an antagonistic interplay between palmitoylation and ubiquitination that regulates protein stability.

Keywords: Hepatocarcinogenesis, S-palmitoylation, ZDHHC20, FASN

Introduction

Post-translational modifications (PTMs) of proteins involve covalent alterations of amino acid side chains that control protein function, subcellular distribution, conformation, and molecular interactions. Hundreds of distinct PTMs are now recognized, encompassing phosphorylation, methylation, acetylation, ubiquitination, glycosylation, and acylation. Protein palmitoylation, a form of acylation, is distinguished by its reversible and dynamic nature [1]. The predominant subtype, S-palmitoylation, involves the covalent linkage of a 16-carbon fatty acid to cysteine residues via thioester bonds. This modification modulates protein architecture, membrane association, stability, maturation, intracellular transport, and functional properties, thereby influencing membrane receptors, ion channels, and diverse (patho)physiological pathways [2]. In mammalian systems, S-palmitoylation is carried out by a family of 23

Access this article online https://smerpub.com/

Received: 17 November 2025; **Accepted:** 02 February 2026

How to cite this article: Schneider N, Frank T, Müller A, Meier C. S-Palmitoylation of FASN by ZDHHC20 Promotes Hepatocellular Carcinogenesis by Preventing Ubiquitin-Mediated Degradation. Arch Int J Cancer Allied Sci. 2026;6(1):39-59. https://doi.org/10.51847/1q9tfBqgAj

zinc-finger aspartate-histidine-histidine-cysteine (ZDHHC) protein acyltransferases (PATs) [2, 3]. Mounting evidence links dysregulated S-palmitoylation to tumor development [4-8]. Numerous proteins have been established as palmitoylation substrates that act as critical mediators in multiple pathologies, especially neurological conditions and malignancies [9-12]. For example, ZDHHC7 and ZDHHC21 facilitate breast cancer cell proliferation by palmitoylating ERα [13, 14]. In glioma, upregulated ZDHHC18 and ZDHHC23 enhance cell survival in the tumor milieu by palmitoylating the proto-oncogene BMI1 (polycomb ring finger) [15]. ZDHHC5-mediated palmitoylation has additionally been correlated with unfavorable outcomes in p53-mutant tumors [16].

Hepatocellular carcinoma (HCC), the predominant and most aggressive primary liver malignancy, exhibits elevated worldwide incidence and mortality owing to its multifaceted etiology and restricted diagnostic and therapeutic modalities [17, 18]. HCC typically arises from iterative liver damage, persistent inflammation, progressive fibrosis, and repeated hepatocyte regeneration [19]. Although substantial advances have been achieved in elucidating HCC pathobiology and treatment strategies, clinical outcomes remain suboptimal [20]. A deeper understanding of the molecular mechanisms governing hepatocarcinogenesis is therefore crucial for discovering reliable early-detection markers and efficacious therapies. Extensive research has connected HCC initiation, metastatic spread, and invasive behavior to dysregulated PTM networks. As one illustration, protein kinase C-delta (PKCδ) stimulates insulin-like growth factor-1 receptor (IGF1R) signaling and augments extracellular regulated protein kinases 1/2 (ERK1/2) activity, thereby accelerating HCC proliferation [21]. Despite these insights, the significance of S-palmitoylation in HCC pathogenesis remains poorly characterized, warranting a systematic examination of the prominent ZDHHC enzymes and their substrate proteins.

ZDHHC20 is a member of the ZDHHC palmitoyltransferase family implicated in multiple biological contexts. Structural analysis by Rana *et al.* [22] revealed the three-dimensional architecture of ZDHHC20 and pinpointed two catalytic sites essential for its palmitoylation activity. This enzyme is overexpressed across several tumor types, and its inhibition has demonstrated therapeutic potential. In breast and lung cancers, ZDHHC20 palmitoylates epidermal growth factor receptor (EGFR); accordingly, ZDHHC20 blockade disrupts EGFR palmitoylation and restrains KRAS-mutant lung adenocarcinoma development [4, 23]. Conversely, in melanoma, ZDHHC20-driven palmitoylation of melanoma cell adhesion molecule (MCAM) supports membrane polarization and augments cellular invasiveness [24]. Additional substrates of ZDHHC20, including YTHDF3, NCAM1, and VAMP7, have been shown to promote pancreatic cancer advancement and metastatic dissemination upon palmitoylation [25, 26]. Feng *et al.* [27] explored ZDHHC20's contributions to metastasis and apoptotic regulation in liver hepatocellular carcinoma (LIHC), emphasizing its clinical and immunological importance in this malignancy.

Crosstalk between oncogenic pathways and lipid metabolism sustains the proliferative, survival, migratory, invasive, and metastatic capabilities of cancer cells [28-35]. Fatty acid synthase (FASN) is a central enzyme that catalyzes de novo fatty acid biosynthesis in mammals. Dysregulated FASN expression or activity supplies tumor cells with essential energy and membrane precursors, thereby supporting malignant progression [36, 37]. Emerging studies on PTM regulation of FASN have identified it as a viable therapeutic target for lipid-metabolism disorders such as obesity, non-alcoholic fatty liver disease (NAFLD), and HCC [38-41]. Strong evidence implicates the acetyl-CoA carboxylase (ACC)/FASN axis as a key driver of hepatocarcinogenesis. Li *et al.* [42] established that FASN is required for AKT-mediated liver tumor formation. Hu *et al.* [43] demonstrated that coordinated AKT and c-Met activation accelerates HCC through mTORC1-dependent FASN upregulation. Separate work has highlighted ACC's involvement in cellular redox balance and viability [44]. These observations support pharmacological targeting of FASN as a promising intervention for HCC. Multiple PTMs regulate FASN, including ubiquitination, SUMOylation, and acetylation. Ubiquitination is particularly critical for controlling FASN abundance, with degradation mediated by the E3 ligase tripartite motif containing 28 (TRIM28) [45]. Hu *et al.* [45] further showed that sorting nexin 8 (SNX8) facilitates FASN turnover by recruiting TRIM28 and enhancing TRIM28-FASN association, thereby suppressing NAFLD progression. These findings illustrate the central importance of FASN signaling in the pathophysiology of liver disease. Continued

investigation into context-specific FASN regulation may reveal novel anti-cancer opportunities.

This investigation reveals that ZDHHC20 deficiency in mice confers protection against chemically induced hepatocarcinogenesis. ZDHHC20 directly palmitoylates FASN at cysteine residues 1471 and 1881, thereby stabilizing the enzyme by interfering with its ubiquitin-proteasome degradation orchestrated by the SNX8-TRIM28 complex. Interference with this ZDHHC20-dependent palmitoylation attenuates HCC development in murine models, establishing ZDHHC20 as a crucial driver of HCC tumorigenesis and progression. Collectively, these observations position ZDHHC20 as a potential biomarker and therapeutic target for HCC.

Materials and Methods

Mice

All animal studies, encompassing experimental designs and protocols, received formal approval from the Animal Ethical and Welfare Committee of Tianjin Medical University Cancer Institute and Hospital (approval number LLSP2019001) and the Laboratory Animal Use Management and Welfare Ethics Committee of Chongqing University Cancer Hospital (approval number CQCH-LAE-A0000202015). Throughout the experiments, mice were maintained in a specific pathogen-free environment, housed five per cage, at a constant temperature of 25 °C and relative humidity of 50% ± 10%, under a standard 12-hour light/dark cycle with lights activated at 8 am. Animals had ad libitum access to standard chow and drinking water.

Zdhhc20−/− knockout mice were generated by Shanghai Model Organisms Center, Inc. (Shanghai, China) employing the CRISPR/Cas9 genome editing approach.

Treatment of mice

For the DEN-induced HCC model, 2-week-old Zdhhc20+/+ or Zdhhc20−/− mice received one intraperitoneal administration of DEN at a dose of 40 mg/kg and were euthanized at 40 weeks of age [46].

In the DEN plus CCl4 HCC model, 2-week-old Zdhhc20+/+ or Zdhhc20−/− mice were first given a single intraperitoneal injection of DEN (20 mg/kg). This was followed by twice-weekly intraperitoneal injections of CCl4 (5 μl/g body weight, prepared as a 20% solution in olive oil) until the study endpoint. Mice were euthanized at either 20 weeks (male littermates) or 22 weeks of age (female littermates), in accordance with previously reported methodologies [47, 48].

Histopathological analysis

Standard protocols were followed for hematoxylin and eosin (H&E) staining and immunohistochemistry (IHC) procedures [49]. Tissue specimens were fixed in 4% paraformaldehyde, dehydrated through a graded series of ethanol concentrations (70–100%), embedded in paraffin blocks, and sectioned at a thickness of 4 μm with a rotary microtome. Prepared sections were stained with H&E and Oil Red O (Sigma). Assessment of proliferative activity was conducted via IHC using a Ki-67-specific antibody (Servicebio, GB111499).

Cell lines and cell culture

The cell lines HEK293T, Huh7, HCCLM3, Hep3B, and HepG2 were sourced from the American Type Culture Collection (ATCC). All lines were verified by short tandem repeat (STR) profiling and routinely screened for *Mycoplasma*. HEK293T, Huh7, HCCLM3, and Hep3B cells were propagated in Dulbecco's modified Eagle medium (DMEM) containing 10% fetal bovine serum (FBS), 100 U/ml penicillin, and 100 mg/ml streptomycin, incubated at 37 °C with 5% CO_2. HepG2 cells were maintained in minimum essential medium supplemented with non-essential amino acids (MEM with NEAA) plus 10% FBS, 100 U/ml penicillin, and 100 mg/ml streptomycin under identical incubation conditions.

Construction of plasmids and establishment of stable cell lines

The following plasmids were obtained from MIAOLING Biology (Wuhan, China): Flag-Vector, Flag-FASN, HA-Vector, HA-FASN, Flag-ZDHHC20, HA-ZDHHC20, Myc-SNX8, His-TRIM28, and Flag-TRIM28. GENEWIZ (Suzhou, China) supplied the control shRNA and ZDHHC20-targeting shRNAs (shRNAZDHHC20-1, shRNAZDHHC20-2, and shRNAZDHHC20-3). Mutants of FASN (C1471S, C1881S, and double C1471/1881S) were generated by introducing point mutations into the Flag-FASN plasmid. The mutagenesis primers were as follows: C1471S mutant — forward: GGGAACCGCCTCCGGTCTGTGCTGCTCTCC, reverse: GTTGGAGAGCAGCACAGACCGGAGGCGGTTC; C1881S mutant — forward: CATCTCCAAGACCTTCAGTCCGGCCCACAAG, reverse:

TGTAGCTCTTGTGGGCCGGACTGAAGGTCTTGG. Site-directed mutagenesis was executed with the Mut Express II Fast Mutagenesis Kit V2 (Vazyme). Target plasmids were first amplified using Phanta Max Super-Fidelity DNA Polymerase. Amplified products were digested with DpnI (1 µl DpnI added, followed by incubation at 37 °C for 1–2 hours) to eliminate the original template. Purified products were then recombined using ExoNase II in 5 × CE II Buffer at 37 °C for 30 minutes, then placed on ice. The recombination mixture (10 µl) was transformed into 100 µl of DH5α competent cells. All resulting constructs were confirmed by Sanger sequencing. Plasmid transfection was performed using Lipofectamine 2000 (Life Technologies) according to the manufacturer's instructions.

Lentiviral particles were produced in HEK293T cells by co-transfection of transfer plasmids (plv-FLAG-FASN, plv-FLAG-FASN C1471S, plv-FLAG-FASN C1881S, or plv-FLAG-FASN C1471/1881S) together with packaging plasmids pMDLg/pRRE and pRSV-Rev (1:1 ratio) and the envelope plasmid pMD2.G, using polyethyleneimine. Collected viral supernatants were stored at 4 °C. Target HCC cells were transduced with the lentiviral preparations and subsequently maintained under puromycin selection for 4–7 days to generate stable cell lines expressing the desired FASN constructs for further analyses.

Cell transfection

Transient transfection was initiated when cells reached 60–70% confluence after overnight attachment. The procedure was performed using Lipofectamine 2000 (Invitrogen) according to the manufacturer's instructions. Successful transfection was verified through Western blotting or quantitative real-time polymerase chain reaction (qRT-PCR).

RNA isolation, reverse transcription, and qRT-PCR

Total RNA was extracted from the samples using TRIzol Reagent (Life Technologies) according to the manufacturer's instructions. Reverse transcription of the purified RNA into cDNA was carried out using Oligo d(T) primers together with SuperScript II reverse transcriptase (Life Technologies). The synthesized cDNA served as the template for quantitative real-time PCR on a StepOnePlus Real-Time PCR System (Applied Biosystems) using SYBR Green PCR master mix and primers specific to the target genes.

Sample preparation and palmitoylation liquid chromatography-mass spectrometry (LC-MS) analysis

Tissues were first weighed and rinsed twice with ice-cold PBS before being ground to a fine powder in liquid nitrogen. Around 50 mg of this powder was then suspended in 200 µL of lysis buffer containing 4% SDS and 150 mM Tris-HCl at pH 8.0. Cell pellets were lysed directly in the same volume of lysis buffer. All preparations were sonicated for 2 minutes in a chilled water bath. Following sonication, proteins were recovered through centrifugation, and their concentrations were measured by the BCA method. For each sample, 3 mg of protein was precipitated using pre-chilled acetone. Free thiol groups on cysteines were blocked by incubating the samples for 12 hours at 4 °C in a total volume of 5 mL PBS containing 0.5% SDS, 1% Triton X-100 (Sigma-Aldrich), protease inhibitors (Thermo Scientific), 5 mM EDTA, and 25 mM N-ethylmaleimide (NEM, Thermo Scientific). Excess NEM was eliminated via chloroform/methanol precipitation. The recovered proteins were redissolved in 1.5 ml of resuspension buffer (4% SDS, protease inhibitors, and 5 mM EDTA in PBS at pH 7.4). This solution was combined with 3 ml of 1 M hydroxylamine (pH adjusted to 7.4 using NaOH; Thermo Scientific) and 500 µl of 4 mM Biotin-HPDP (Thermo Scientific) dissolved in DMSO, then incubated for 2 hours at 25 °C with mild agitation. After a further precipitation step, proteins were solubilized in 6 M urea, diluted six times with 50 mM ammonium bicarbonate, and subjected to trypsin digestion at a 1:50 enzyme-to-protein ratio for 20 hours at 37 °C. The resulting peptides were desalted on C18 spin columns (Thermo Scientific). Dried peptides were reconstituted in 200 µl of loading buffer (0.2% SDS, 0.2% Triton X-100, and 500 mM NaCl) and incubated with 100 µl of high-capacity streptavidin beads (Thermo Scientific) for 2 hours at ambient temperature. The beads underwent three washes with 5 ml PBS containing 0.2% SDS, 0.2% Triton X-100, and 500 mM NaCl, followed by two additional washes with 1 ml PBS. Elution of captured peptides was achieved by incubating the beads in 0.2 ml of elution buffer (50 mM NH_4HCO_3 containing 10 mM TCEP) for 2 hours at room temperature. The collected eluate was treated with 50 mM iodoacetamide to alkylate the previously palmitoylated cysteines. Finally, peptides were desalted using C18 Stage Tips and prepared for LC-MS/MS.

NanoLC-MS/MS analysis was conducted using a Q Exactive HF-X mass spectrometer (Thermo Scientific) connected to an Easy nLC 1200 liquid chromatography system. Peptides were loaded onto a reverse-phase C18 column (20 cm × 75 µm ID, 2 µm particles; Dr. Maisch GmbH, Germany) equilibrated with buffer A (2% ACN, 0.1% FA). Separation occurred via a 120-minute linear gradient of buffer B (90% ACN, 0.1% FA) delivered at 300 nl/min with the following profile: 0–2 min (2–5% B), 2–82 min (5–20% B), 82–100 min (20–35% B), 100–112 min (35–90% B), and 112–120 min (held at 90% B).

Mass spectrometric data were acquired in positive-ion mode using a nanoelectrospray ionization source operated at 2.1 kV. Survey full MS scans covered the m/z range 350–1800 at 60,000 resolution (at m/z 200), using an AGC target of 3e6 and a maximum ion injection time of 50 ms. Internal mass calibration was maintained with a lock mass at 445.120025 Da. The top 20 most intense precursor ions were selected for fragmentation by higher-energy collisional dissociation (HCD) at a normalized collision energy of 28. MS/MS spectra were recorded at 15,000 resolution (at m/z 200) with an AGC target of 1e5 and maximum injection time of 50 ms. Precursor isolation width was 1.6 Th, and dynamic exclusion was set to 30 seconds.

Acyl-biotin exchange assay (ABE)

The acyl-biotin exchange (ABE) method was applied to detect FASN palmitoylation status following a previously validated protocol [50]. In short, total proteins extracted from cells were incubated with NEM at 4 °C for 1 hour under continuous mixing. The protein of interest was then immunoprecipitated using a specific antibody conjugated to magnetic beads. After purification, the immunoprecipitated material was treated with 1 M hydroxylamine (HAM, pH 7.2) for 1 hour at room temperature. Subsequently, the sample was labeled with 5 µM biotin-BMCC at 4 °C for 2 hours. The bead-bound complexes were resuspended in 40 µl SDS sample buffer, boiled for 10 minutes at 100 °C, and analyzed by Western blotting.

Protein extraction and Western blot analysis

Following three washes with ice-cold PBS, cellular proteins were extracted in RIPA lysis buffer (Beyotime, P0013K) supplemented with phenylmethanesulfonyl fluoride (PMSF) and a cocktail of protease inhibitors. Lysis was performed on ice for 30 minutes. The lysates were further disrupted by sonication and clarified by centrifugation at 12,000 g for 20 minutes at 4 °C. Protein concentrations in the cleared supernatants were determined with the BCA Protein Assay Kit (Pierce, 23227) per the manufacturer's recommendations. Aliquots containing 30–50 µg of total protein per lane were separated by SDS-polyacrylamide gel electrophoresis (SDS-PAGE) and transferred to membranes for immunoblotting. Detection was performed using UltraSignal Supersensitive ECL chemiluminescent substrate (4A Biotech, 4AW011-1000).

Immunoprecipitation (IP) assay

For immunoprecipitation and co-immunoprecipitation studies, cells were subjected to the indicated transfections and treatments, then rinsed three times with ice-cold PBS. Lysis was performed on ice for 30 minutes using Western/IP lysis buffer (Beyotime, P0013J) supplemented with PMSF and a protease inhibitor cocktail. Lysates were disrupted by sonication and clarified by centrifugation at 12,000 g for 20 minutes at 4 °C. Protein concentrations were quantified with the BCA Protein Assay Kit (Pierce, 23227) per the manufacturer's guidelines. An aliquot corresponding to 150 µg of protein was reserved as the "input" sample. The remaining lysates, containing equal amounts of protein, were incubated with protein A/G magnetic beads (Pierce, 26162) preconjugated with the target antibody. Following incubation for at least 8 hours, the beads were washed three times with lysis buffer. Captured proteins were released by boiling in 1 × SDS-PAGE loading buffer and analyzed by Western blotting using the standard procedure.

Immunofluorescence microscopy

In brief, 60,000 cells were plated onto coverslips and cultured overnight at 37 °C under 5% CO_2. After the relevant transfections or treatments, cells were washed three times with ice-cold PBS, fixed in 4% paraformaldehyde, and permeabilized with 0.3% Triton X-100 in PBS. Nonspecific binding sites were blocked with 5% bovine serum albumin in PBS. Samples were then incubated sequentially with primary and secondary antibodies. Nuclei were stained with DAPI, and coverslips were mounted with ProLong Diamond anti-fade reagent (Invitrogen, P36971). Confocal images were obtained using a Leica STELLARIS 5 microscope.

Ubiquitination assays

Cells reaching 80% confluence were transfected with the designated expression constructs. Forty-eight hours later, cells were treated with 10 μM MG132 (MedChemExpress, HY-13259) for 6 hours. Cells were subsequently lysed in RIPA buffer, sonicated, and centrifuged at 12,000 g for 20 minutes at 4 °C. Protein concentrations were measured using the BCA Protein Assay Kit (Pierce, 23227), with 150 μg of protein reserved as the "input". Equal amounts of protein were incubated overnight with protein A/G magnetic beads (Pierce, 26162) pre-bound to the appropriate antibody. The precipitated material was eluted in 1 × SDS-PAGE loading buffer and examined by immunoblotting.

Protein half-life assay

Protein turnover was assessed by adding 100 μg/ml cycloheximide (CHX) (Abmole, M4879) to the culture medium. Cells were harvested at selected time points following CHX treatment, and protein levels were quantified via Western blot analysis.

Protein-protein docking

The amino acid sequences for human ZDHHC20 (UniProt ID: Q5W0Z9) and FASN (UniProt ID: P49327) were obtained from the UniProt database. Protein-protein docking simulations between ZDHHC20 and FASN were executed using the HDOCK platform. Prepared structures were submitted for global rigid-body docking with default parameters. The model with the lowest binding energy was selected, and the resulting interaction interface was visualized in PyMOL.

CCK-8 assay

Cell proliferative capacity was determined using the CCK-8 assay according to the manufacturer's protocol. Logarithmically growing cells were seeded at 2000 cells per well in 200 μl medium into 96-well plates and allowed to adhere overnight. At specified intervals, CCK-8 reagent was added, and plates were incubated for 2 hours at 37 °C. Absorbance readings at 450 nm were recorded using a microplate reader in the dark.

Colony formation assay

A colony formation assay evaluated long-term cell survival. Logarithmically growing cells were seeded into 6-well plates at a density of 500 cells per well in 2 mL medium. After 10–14 days of culture, colonies were fixed with methanol for 20 minutes, stained with 1% crystal violet for 15 minutes, rinsed four times with water, and air-dried. Colonies containing more than 50 cells were scored as positive.

Statistical analysis

Data analysis was performed using SPSS 26.0 and GraphPad Prism 8. Results are reported as mean ± standard deviation (SD). Comparisons between two groups were conducted using unpaired two-tailed Student's t-tests or the Mann-Whitney U test where appropriate. A p-value less than 0.05 was considered statistically significant (*P < 0.05, **P < 0.01).

Results and Discussion

ZDHHC20 is highly expressed in HCC tissues and negatively correlated with prognosis

This investigation aimed to comprehensively profile the expression of ZDHHC family palmitoyltransferases in hepatocellular carcinoma (HCC) and to identify the most prominent member, while clarifying the role of protein palmitoylation in HCC pathogenesis. Candidate ZDHHC enzymes were screened by integrating mRNA and protein expression data from the Human Protein Atlas (HPA) database with survival information from the The Cancer Genome Atlas (TCGA) database, and the results were analyzed using the Gene Expression Profiling Interactive Analysis (GEPIA) tool. Examination of mRNA abundance across HCCLM3, Hep3B, and Huh7 cell lines revealed the five highest expressed members as ZDHHC6, ZDHHC4, ZDHHC20, ZDHHC21, and ZDHHC5. Immunohistochemistry data from the HPA database further categorized ZDHHC proteins according to expression intensity into weak and strong groups, with ZDHHC12, ZDHHC9, ZDHHC21, ZDHHC20, and ZDHHC15 showing the strongest signals. Survival analysis using TCGA data identified ZDHHC20, ZDHHC7, ZDHHC16, ZDHHC9, and ZDHHC15 as the top five enzymes most closely linked to overall survival outcomes in HCC. Overlap analysis of these three independent rankings via Venn diagram consistently highlighted ZDHHC20 as the enzyme most strongly associated with HCC. TCGA cohort analysis additionally confirmed markedly higher ZDHHC20 transcript levels in tumor tissues than in adjacent normal liver. Elevated ZDHHC20 protein expression correlated with poorer disease-free survival and reduced progression-free survival. These observations motivated detailed functional studies of ZDHHC20 in HCC. Functional assays, including colony formation and CCK-

8, demonstrated that forced ZDHHC20 expression significantly enhanced HCC cell growth, whereas its depletion inhibited proliferation. Consistent with these in vitro findings, stable ZDHHC20 overexpression accelerated tumor progression in a subcutaneous cell-derived xenograft (CDX) model. Overall, the evidence supports ZDHHC20 as a critical promoter of HCC development and a marker of poor clinical outcome.

ZDHHC20−/− mice show reduced HCC formation induced by chemical agents

Considering the overexpression and unfavorable prognostic value of ZDHHC20 in human HCC, its pathophysiological role was investigated using genetically modified mice. The CRISPR/Cas9 system was employed to delete a 2268 bp segment encompassing the third exon of the Zdhhc20 locus in the C57BL/6J background. Homozygous Zdhhc20 knockout mice were obtained after two generations of breeding. Successful genotyping of Zdhhc20+/+, Zdhhc20+/−, and Zdhhc20−/− animals was verified by PCR using two primer sets. Absence of Zdhhc20 mRNA in liver tissue was confirmed. Two standard chemically induced HCC models were subsequently established: DEN alone and the combination of DEN with CCl4 **(Figure 1a)**. Both models included male and female cohorts. Macroscopic liver appearances are displayed in **Figures 1b and 1f**. Histopathological evaluation by H&E staining showed disrupted hepatic architecture characterized by varying degrees of hepatocyte edema, degeneration, necrosis, inflammatory cell infiltration, atypical hyperplasia, loss of normal lobular organization, and peripheral lesions. Neoplastic hepatocytes exhibited disordered arrangement, nuclear hyperchromasia, marked pleomorphism, and visible mitotic activity **(Figure 1c)**. Tumor incidence was dramatically lower in Zdhhc20−/− mice than in wild-type littermates **(Figure 1d)**. Quantitative assessment further revealed that Zdhhc20+/+ mice formed significantly more and larger tumor nodules compared with Zdhhc20−/− animals **(Figure 1f)**. Serum biochemical indicators of liver damage, including alanine aminotransferase (ALT) and aspartate aminotransferase (AST), were substantially decreased in the knockout group. Levels of pro-inflammatory cytokines interleukin-6 (IL-6) and tumor necrosis factor-α (TNF-α) were similarly reduced relative to wild-type controls. Taken together, these findings indicate that ZDHHC20 deficiency protects against chemical carcinogen-induced hepatocyte injury, inflammation, and subsequent hepatocarcinogenesis.

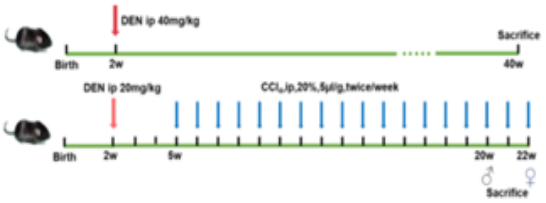

a)

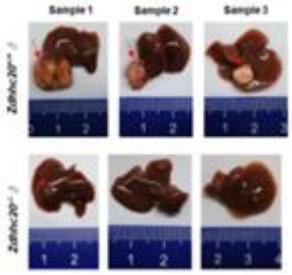

b)

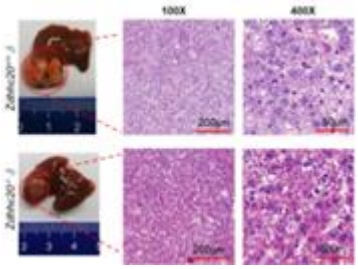

c)

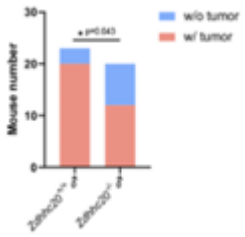

d)

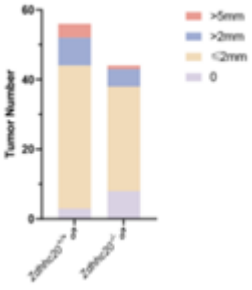

e)

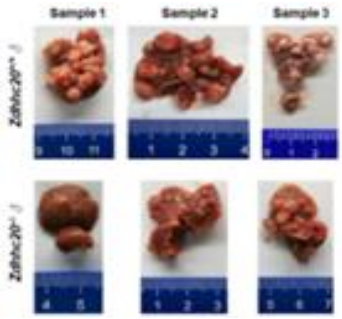

f)

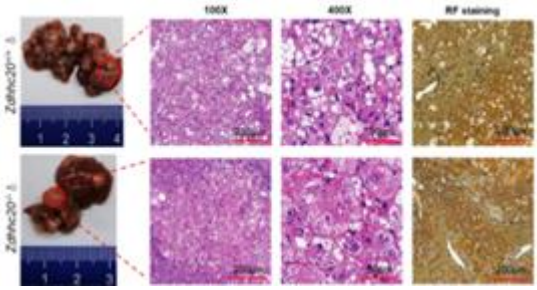

g)

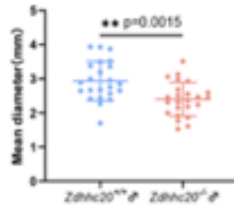

h)

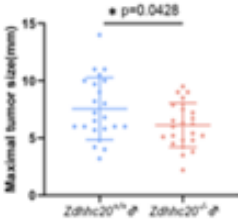

i)

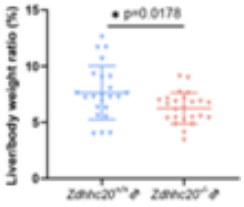

j)

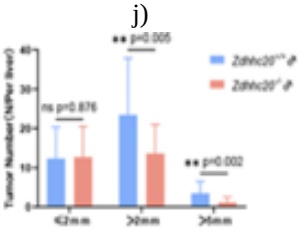

k)

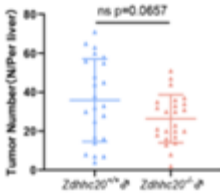

l)

Figure 1. Zdhhc20−/− mice developed fewer liver tumors in chemical-induced HCC models

(a) Schematic illustration of the experimental timelines for the DEN alone and DEN combined with CCl4 HCC induction protocols in mice, (b, c) Typical macroscopic views of livers (b) and representative H&E-stained histological sections (c) from DEN-treated animals of the indicated genotypes. Red arrows highlight HCC nodules. Scale bar = 200 μm–50 μm. (d, e) Number of mice with and without tumors (d) and nodule size distribution (0, ≤ 2, >2, >5 mm) (e) in the DEN-induced HCC model among the specified male cohorts. (f-l) Representative gross liver photographs (f), H&E staining (g), reticular fiber (RF) staining of tumor regions, mean nodule diameter (h), largest nodule diameter (i), liver-to-body weight ratio (j), nodule size distribution (≤ 2, >2, >5 mm) (k), and total tumor counts (l) in the DEN + CCl4 model for the designated male groups. Scale bar = 200 μm–50 μm. DEN, diethylnitrosamine. Data are presented as mean ± SD. ns, no significance; *P < 0.05, **P < 0.01, ***P < 0.001; unpaired two-tailed Student's t-tests and non-parametric Mann-Whitney test were applied.

In the DEN + CCl4 model, recognized for its close resemblance to the pathogenic processes observed in human HCC **(Figure 1a)**, Zdhhc20−/− mice displayed substantially diminished tumor formation **(Figure 1f)**. Histopathological assessment via H&E and reticular fiber (RF) staining revealed more advanced malignant transformation and pronounced fibrotic changes in the livers of Zdhhc20+/+ mice. These features included severe disruption of lobular architecture, increased collagen accumulation surrounding central veins and in portal regions, abundant infiltration of inflammatory cells and fibroblasts in fibrous bands, hepatocyte pleomorphism with swelling, degeneration, necrosis, enlarged and hyperchromatic nuclei, and frequent pathological mitoses **(Figure 1g)**. Proliferative index, as measured by Ki-67 immunohistochemistry, was higher in tumors arising in Zdhhc20+/+ mice. In male mice, notable differences were recorded for mean tumor diameter **(Figure 1h)**, maximum tumor diameter **(Figure**

1i), liver-to-body weight ratio **(Figure 1j)**, and the numbers of nodules in the size ranges of less than 2 mm, greater than 2 mm, and greater than 5 mm **(Figure 1k)**. Total nodule count, however, showed no significant variation between genotypes **(Figure 1l)**. In female mice, significant genotype-dependent differences emerged in total nodule number, maximum nodule diameter, liver-to-body weight ratio, and nodule size distribution. However, mean nodule diameter remained comparable. These observations collectively indicate that deletion of ZDHHC20 ameliorates hepatic injury and thereby restrains HCC progression. To examine potential effects on the early phases of disease, an acute DEN-induced liver injury model was utilized, which reflects the inflammatory conditions preceding HCC. Eight-week-old mice were administered a single intraperitoneal dose of 100 mg/kg DEN and sacrificed 48 hours later. Zdhhc20+/+ mice showed markedly elevated serum ALT and AST activities compared with Zdhhc20−/− littermates. Oil Red O staining demonstrated greater hepatic damage in wild-type animals, which also experienced more pronounced body weight reduction. Liver-to-body weight ratios did not differ significantly between groups. These experiments reveal that ZDHHC20 ablation effectively shields mice from acute DEN-triggered hepatotoxicity and inflammation, as well as from chronic CCl4-mediated injury and fibrogenesis. In summary, the results underscore the critical role of ZDHHC20 in promoting chemically induced hepatocarcinogenesis.

Proteomic examination of palmitoylation identifies the fatty acid metabolic pathway and substrates of ZDHHC20

To identify the protein substrates modified by ZDHHC20 through palmitoylation during HCC development, liquid chromatography-tandem mass spectrometry (LC-MS/MS)-based palmitoylation profiling was performed on mouse HCC tissue samples **(Figure 2a)**. In comparison with the Zdhhc20+/+ controls, the Zdhhc20−/− group displayed markedly lower palmitoylation on 97 proteins involving 123 cysteine residues **(Figures 2b and 2c)**. Bubble plots from Gene Ontology (GO) enrichment analysis of the top 20 biological processes, combined with KEGG pathway enrichment results, revealed that fatty acid metabolism was prominently disrupted by ZDHHC20 ablation **(Figures 2d and 2e)**.

The contribution of ZDHHC20 to fatty acid metabolism was further explored by assessing transcriptional correlations between ZDHHC20 and associated metabolic regulators in HCC via the GEPIA database. Strong positive associations were detected with SREBP1, GPAT, ACLY, ACC, LPIN1, ELOVL1, and FADS2, while DGAT1 and FASN mRNA levels showed no meaningful relationship. In agreement with these observations, quantitative RT-PCR performed on liver tissues from DEN + CCl4-treated mice confirmed that ZDHHC20 deletion suppressed mRNA expression of Srebp1, Gpat, Acly, Acc, Lpin1, Elovl1, and Fads2, but had no impact on Fasn transcript levels **(Figure 2f)**.

Next, transcript levels of central genes regulating cholesterol biosynthesis and export, fatty acid import, and de novo fatty acid synthesis were quantified. ZDHHC20 overexpression in HCC cells produced pronounced increases in CYP7A1, FABP-1, CD36, SREBP1, ACC1, and ACC2 mRNA. Conversely, HMGCR, FATP1, and FASN expression remained essentially unchanged **(Figure 2g)**. In addition, elevated ZDHHC20 expression increased intracellular total cholesterol and triglyceride content **(Figures 2h and 2i)**, whereas its suppression led to reciprocal reductions **(Figures 2j and 2k)**.

Protein-level analyses similarly demonstrated links between ZDHHC20 and key lipid regulators. Overexpression of ZDHHC20 enhanced ACC and SREBP1 protein abundance, with knockdown exerting the opposite influence. A dietary metabolic model was also established by providing mice with a high-fat, high-sugar diet commencing at eight weeks of age. Zdhhc20−/− animals exhibited attenuated body weight gain relative to Zdhhc20+/+ littermates. Taken together, these data affirm that ZDHHC20 modulates fatty acid metabolism and thereby facilitates HCC progression.

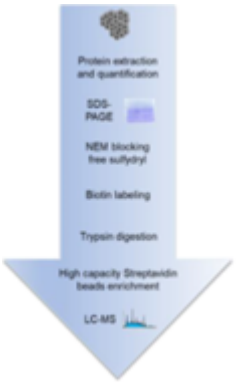

a)

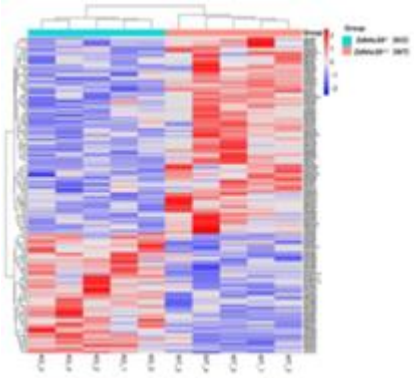

b)

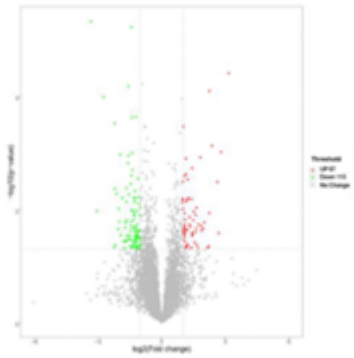

c)

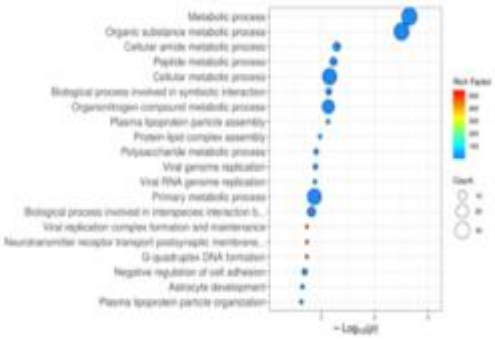
Metabolic process
Organic substance metabolic process
Cellular amide metabolic process
Peptide metabolic process
Cellular metabolic process
Organonitrogen compound metabolic process
Plasma lipoprotein particle assembly
Protein-lipid complex assembly
Polysaccharide metabolic process
Viral genome replication
Viral RNA genome replication
Primary metabolic process
Astrocyte development
Plasma lipoprotein particle organization
Rich Factor
Count

d)

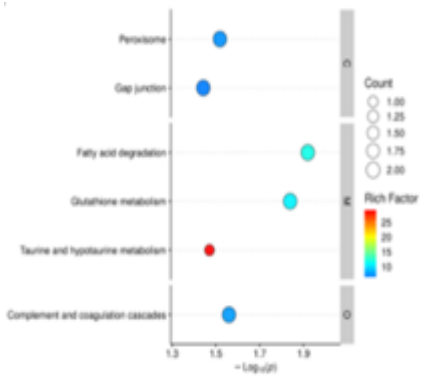
Peroxisome
Gap junction
Fatty acid degradation
Glutathione metabolism
Taurine and hypotaurine metabolism
Complement and coagulation cascades
Count
Rich Factor

e)

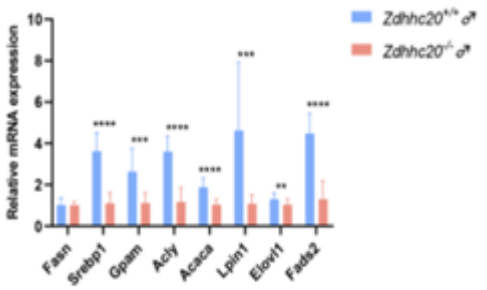
Zdhhc20+/+ ♂
Zdhhc20-/- ♂
Relative mRNA expression
Fasn
Srebp1
Gpam
Acly
Acaca
Lpin1
Elovl1
Fads2

f)

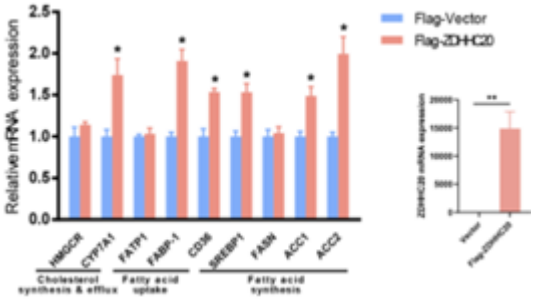
Flag-Vector
Flag-ZDHHC20
Relative mRNA expression
HMGCR
CYP7A1
FATP1
FABP-1
CD36
SREBP1
FASN
ACC1
ACC2
Cholesterol synthesis & efflux
Fatty acid uptake
Fatty acid synthesis

g)

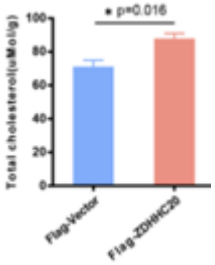
p=0.016
Total cholesterol(uMol/g)
Flag-Vector
Flag-ZDHHC20

h)

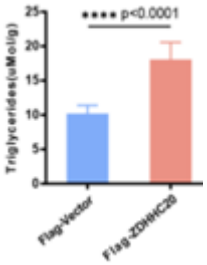
p<0.0001
Triglycerides(uMol/g)
Flag-Vector
Flag-ZDHHC20

i)

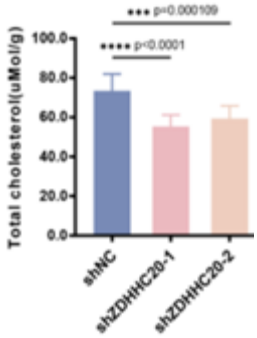
p=0.000109
p<0.0001
Total cholesterol(uMol/g)
shNC
shZDHHC20-1
shZDHHC20-2

j)

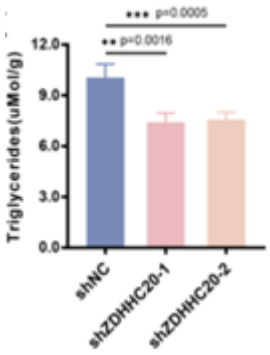

k)

Figure 2. Functional annotation of the modified palmitoylation proteome following ZDHHC20 knockout

(a) Workflow of palmitoylation LC-MS analysis (n = 5 biological replicates), (b, c) Heatmap and volcano plot illustrating differentially palmitoylated protein sites. (d, e) GO (Gene Ontology) analysis (d) and KEGG (Kyoto Encyclopedia of Genes and Genomes) pathway analysis (e) of palmitoylated proteins from mouse HCC tissues. BP: Biological Process, CC: Cellular Component, MF: Molecular Function, (f) Relative mRNA expression of genes participating in the hepatic de novo lipogenesis pathway in mouse HCC tissues, (g) Relative mRNA expression of selected lipid metabolism-related genes in HepG2 cells following transfection with empty vector or Flag-tagged ZDHHC20 plasmid, (h, i) Total cholesterol (h) and triglyceride (i) concentrations in HepG2 cells transfected with vector or Flag-tagged ZDHHC20 plasmid. (j, k) Total cholesterol (j) and triglyceride (k) concentrations in HepG2 cells transfected with shNC or shZDHHC20 plasmid.

ZDHHC20 interacts with FASN and mediates FASN palmitoylation

Since the liver functions as the body's primary metabolic center and a key site for fatty acid processing, it was proposed that ZDHHC20 contributes to HCC development by attaching palmitoyl groups to essential molecules in the fatty acid metabolic cascade. After data normalization and quantitative assessment via palmitoylation LC-MS/MS, 123 palmitoylation sites distributed across 97 proteins showed significant reduction in the ZDHHC20 knockout samples. Of these, FASN showed the largest shift among proteins involved in fatty acid metabolism. Therefore, efforts were made to confirm the association between ZDHHC20 and FASN.

For this purpose, exogenous ZDHHC20 and FASN were introduced simultaneously into three different HCC cell lines. Co-immunoprecipitation (co-IP) experiments confirmed a direct interaction between ZDHHC20 and FASN **(Figure 3a)**. In addition, endogenous FASN interacted with introduced ZDHHC20 **(Figure 3b)**. Immunofluorescence studies further revealed that endogenous and/or exogenous ZDHHC20 and FASN proteins co-localized within HCC cells **(Figures 3c and 3d)**.

To confirm FASN palmitoylation in HCC cells, the IP-ABE technique was applied, demonstrating clear palmitoylation signals for both endogenous FASN and transfected Flag-FASN **(Figures 3e and 3f)**. Application of the general palmitoylation inhibitor 2-bromopalmitate (2-BP) led to a sharp decline in FASN palmitoylation, verifying that the modification involves S-palmitoylation via thioester bonds **(Figure 3g)**. Additional IP-ABE experiments indicated that depletion of ZDHHC20 substantially lowered FASN palmitoylation levels **(Figure 3h)**. At the same time, increased expression of ZDHHC20 produced a notable enhancement in the palmitoylation signal **(Figure 3i)**. These results collectively establish that ZDHHC20 binds to FASN and acts as the palmitoyltransferase responsible for its modification.

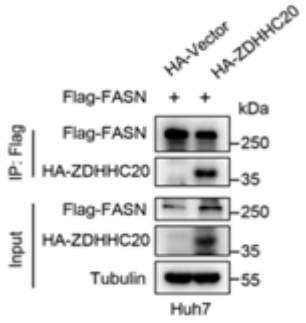

a)

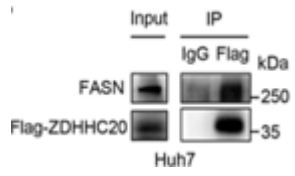

b)

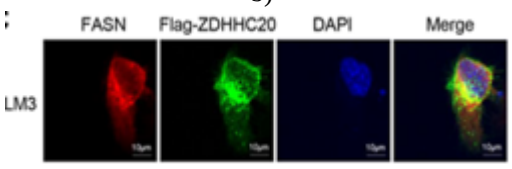

c)

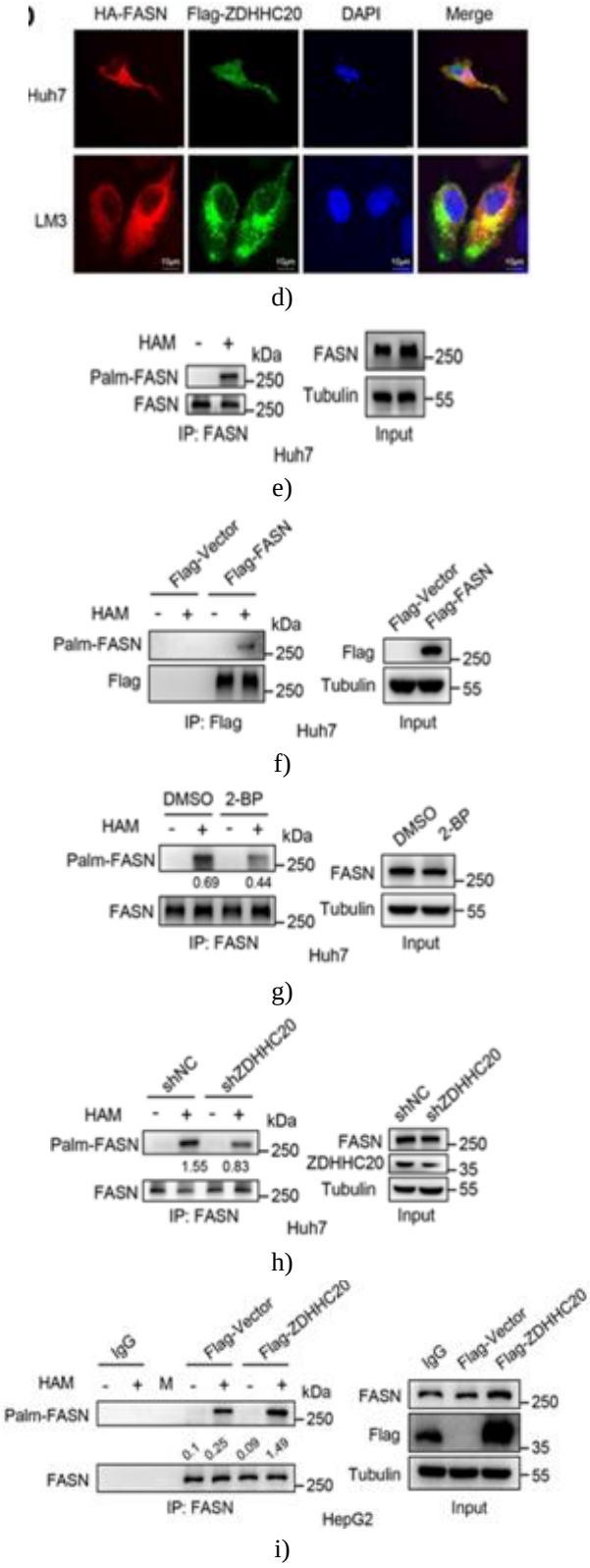

Figure 3. The palmitoyltransferase ZDHHC20 associates with FASN and regulates its palmitoylation

(a) Lysates prepared from Huh7 cells co-transfected with Flag-tagged FASN and HA-tagged ZDHHC20 plasmids were subjected to immunoprecipitation with Flag, HA, or control IgG antibodies, followed by immunoblotting with the specified antibodies to verify protein-protein interactions, (b) Lysates from Huh7 cells expressing Flag-ZDHHC20 were immunoprecipitated using Flag or IgG antibodies and analyzed by immunoblotting to detect interactions, (c) Immunofluorescence imaging of FASN and Flag-tagged ZDHHC20 in HCCLM3 cells, with DAPI nuclear counterstaining. Scale bar = 10 μm. (d) Immunofluorescence detection of exogenous FASN and ZDHHC20 proteins in HCCLM3 and Huh7 cells, with DAPI nuclear staining. Scale bar = 10 μm. (e, f) Palmitoylation of endogenous FASN and Flag-tagged FASN in Huh7 cells was determined using the ABE method and visualized by streptavidin-HRP immunoblotting. HAM+: HAM present; HAM-: HAM absent, (g) Huh7 cells were treated with 50 μM 2-bromopalmitate (2-BP) for 8 h before ABE analysis, (h) Palmitoylation levels of endogenous FASN were examined by ABE assay in Huh7 cells following transfection with shNC or shZDHHC20 constructs, and (i) Palmitoylation of endogenous FASN was assessed by ABE assay in Huh7 cells after transfection with empty vector or Flag-tagged ZDHHC20 plasmid.

ZDHHC20 palmitoylates FASN at cysteines 1471 and 1881

Mass spectrometry analysis of secondary fragments indicated palmitoylation at cysteine positions 1464 and 1874 within mouse FASN **(Figures 4a and 4b)**. These modification sites displayed substantially lower palmitoylation in Zdhhc20−/− animals **(Figure 4c)**. Computational prediction with CSS-Palm software assigned high confidence scores for palmitoylation at the equivalent positions in both human and mouse FASN sequences **(Figure 4d)**. Structural modeling through protein-protein docking demonstrated a clear binding interface between ZDHHC20 and FASN **(Figure 4e)**. The residues C1471 and C1881 are notably conserved among FASN orthologs from various species **(Figure 4f)**.

Cysteine-to-serine substitutions were introduced at these positions **(Figure 4g)**. Compared with the wild-type protein, both individual and combined mutations at these cysteines resulted in markedly attenuated palmitoylation signals **(Figures 4h and 4i)**. These experiments collectively confirm that FASN serves as a substrate for

ZDHHC20-mediated palmitoylation, with cysteines 1471 and 1881 acting as the major acceptor sites.

a)

b)

Protein Position	FC	*P* Value
Q3UHT6-C1464	0.3033	0.0209
Q3UHT6-C1874	0.4945	0.0385

c)

Species	Primary accession	Predicted Candidate Site Cysteine(C)	Amino Acid Sequence	Score	Cutoff
Mus musculus	Q3UHT6	C1464	GGHRIRCLLSNL	0.7153	0.6484
Mus musculus	Q3UHT6	C1874	AISKTFCPAHKSY	0.8657	0.6484
Homo sapiens	P49327	C1471	GGNRLRCVLLSNL	0.8127	0.7766
Homo sapiens	P49327	C1881	AISKTFCPAHKSY	0.8513	0.7766

d)

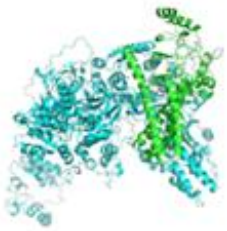

e)

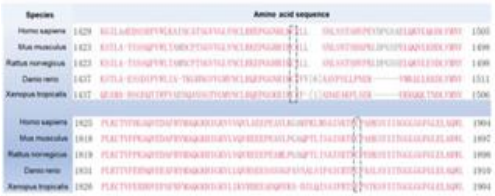

f)

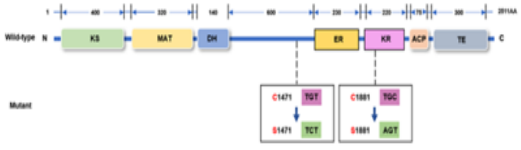

g)

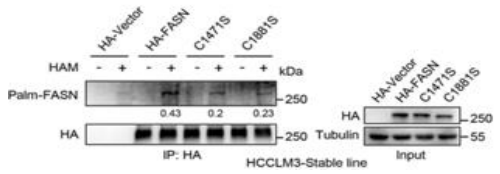

h)

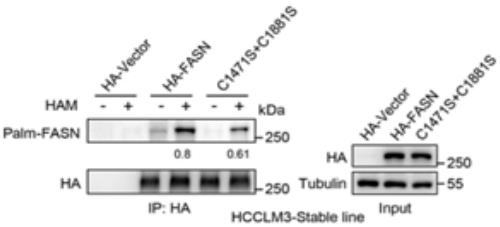

i)

Figure 4. ZDHHC20-dependent palmitoylation of FASN at cysteines 1471 and 1881

(a, b) Altered palmitoylation sites on FASN identified via LC-MS analysis of mouse HCC tissues, (c) Significant palmitoylation sites on FASN detected by LC-MS, (d) Predicted palmitoylation sites on FASN validated using CSS-Palm software, (e) Protein-protein docking model illustrating ZDHHC20 (green) in complex with FASN (blue), (f) Multiple sequence alignment highlighting conservation of FASN across vertebrate species, (g) Diagram of the domain structure of full-length human FASN showing cysteine-to-serine mutations at residues 1471 and 1881, and (h, i) ABE assays conducted on cells expressing HA-Vector, HA-tagged wild-type FASN, or the indicated single (C1471S, C1881S) and double (C1471S + C1881S) mutants.

Palmitoylation of FASN antagonizes its ubiquitination

To investigate the importance of ZDHHC20-driven FASN palmitoylation in HCC pathogenesis, cells were exposed to the palmitoylation inhibitor 2-BP. While this treatment did not alter the intracellular distribution of FASN, it produced a clear reduction in fluorescence intensity. Notably, 2-BP also lowered overall FASN protein abundance. In contrast, inhibitors of depalmitoylation such as ML348 and palmostatin B (Palm B) elevated FASN protein expression. Pulse-chase experiments with cycloheximide (CHX) revealed that 2-BP accelerated FASN turnover, whereas ML348 and Palm B extended its half-life.

To clarify the dominant degradation mechanism, HCCLM3 cells were treated with the proteasome inhibitor MG132 or the lysosomal inhibitors chloroquine and NH4Cl. MG132 effectively blocked CHX-induced

degradation and stabilized FASN, while the lysosomal inhibitors had little effect **(Figures 5a and 5b)**. These data establish the ubiquitin-proteasome system as the principal pathway responsible for FASN turnover in HCC. Blocking palmitoylation with 2-BP led to enhanced ubiquitination of both endogenous and exogenous FASN when proteasome activity was inhibited by MG132 **(Figures 5c and 5d)**. This indicates that palmitoylation stabilizes FASN by limiting its ubiquitination.

Further experiments tested whether ZDHHC20 mediates this effect. Ectopic expression of ZDHHC20 increased FASN protein abundance, as detected by immunoblotting **(Figure 5e)** and immunofluorescence **(Figure 5f)**. In contrast, silencing ZDHHC20 reduced FASN levels. CHX chase assays corroborated that ZDHHC20 knockdown shortened FASN half-life. At the same time, its overexpression prolonged it **(Figures 5g and 5h)**. Consistent with these observations, ZDHHC20 depletion augmented FASN ubiquitination **(Figure 5i)**, whereas ZDHHC20 overexpression diminished it. In conclusion, ZDHHC20-mediated palmitoylation of FASN counteracts its ubiquitination, thereby enhancing protein stability and supporting FASN function during HCC development.

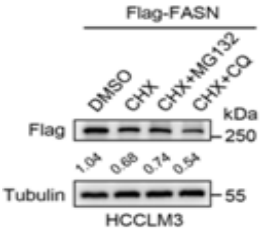

a)

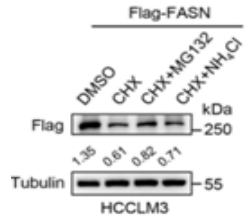

b)

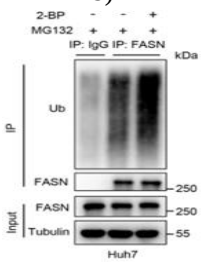

c)

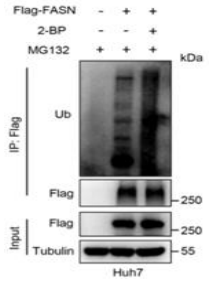

d)

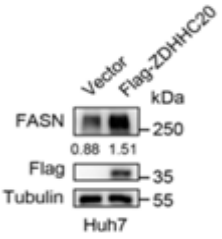

e)

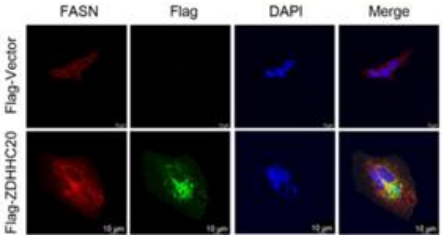

f)

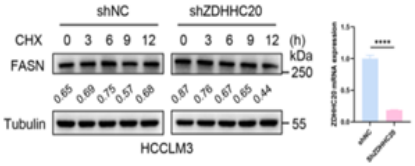

g)

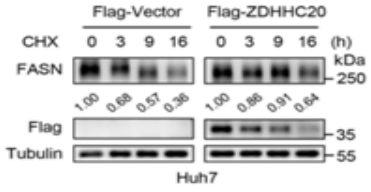

h)

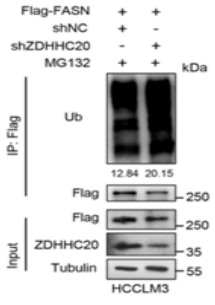

i)

Figure 5. Palmitoylation of FASN antagonizes its ubiquitination modification

(a, b) Levels of Flag-tagged FASN protein were evaluated following 6 h treatment with cycloheximide (CHX, 100 μg/ml) alone or in combination with chloroquine (CQ, 20 μM), NH4Cl (10 μM), or MG132 (10 μM), (c, d) Ubiquitination of endogenous FASN or Flag-tagged FASN was assessed in Huh7 cells pretreated with or without 50 μM 2-bromopalmitate (2-BP) for 24 h, followed by MG132 (10 μM) for 8 h, (e) FASN protein expression in Huh7 cells transfected with a control vector or Flag-tagged ZDHHC20, (f) Immunofluorescence detection of FASN and Flag in Huh7 cells expressing vector or Flag-tagged ZDHHC20. DAPI stains nuclei. Scale bar = 10 μm. (g-h) Stability of endogenous or Flag-tagged FASN protein was monitored under CHX (100 μg/ml) treatment in the indicated experimental groups, and (i) Ubiquitination levels of Flag-tagged FASN were examined in HCCLM3 cells transfected with shZDHHC20.

ZDHHC20-mediated palmitoylation of FASN reduces its degradation via antagonism of the SNX8-TRIM28 complex

Prior investigations have shown that the SNX8-TRIM28 complex associates with FASN and controls its abundance in HCC [45]. To clarify the competitive relationship between palmitoylation and ubiquitination on FASN, it was hypothesized that palmitoylation catalyzed by ZDHHC20 disrupts FASN's association with TRIM28, leading to greater protein stability. This idea was tested by co-expressing Myc-tagged SNX8 with Flag-tagged FASN in Huh7 cells, either alone or in combination with HA-tagged ZDHHC20. Introduction of Myc-tagged SNX8 lowered FASN levels, but co-expression of HA-tagged ZDHHC20 largely reversed this reduction, restoring Flag-tagged FASN abundance **(Figure 6a)**. Parallel experiments with His-tagged TRIM28 yielded comparable outcomes, with HA-tagged ZDHHC20 mitigating the suppressive action of TRIM28 on Flag-tagged FASN **(Figure 6b)**.

Co-immunoprecipitation studies revealed that ZDHHC20 weakened the physical association of SNX8 **(Figure 6c)** and TRIM28 **(Figure 6d)** with FASN. Treatment with 2-BP amplified the ability of TRIM28 and SNX8 to promote FASN degradation **(Figures 6e and 6f)**, whereas Palm B produced the opposing outcome. These observations collectively establish that palmitoylation of FASN, driven by ZDHHC20, directly competes with ubiquitination mediated by the SNX8-TRIM28 complex **(Figure 6g)**.

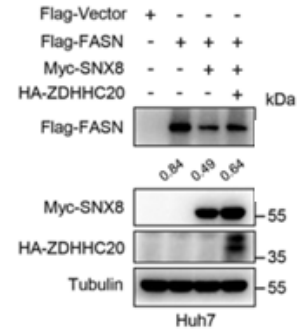

a)

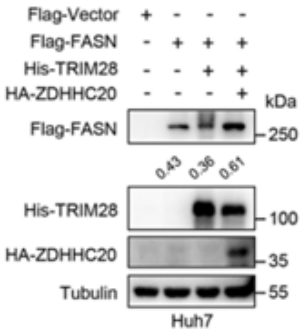

b)

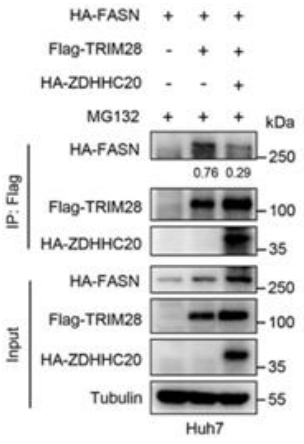

c)

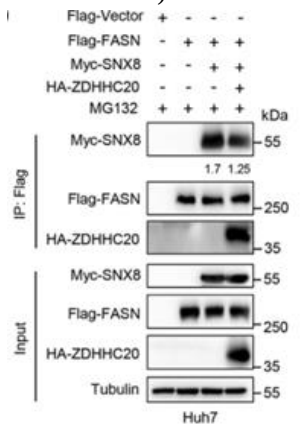

d)

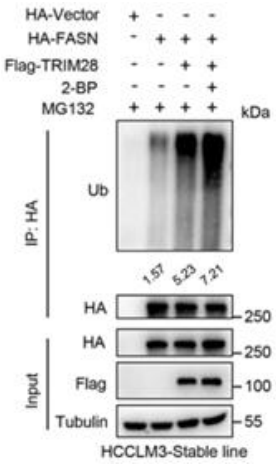

e)

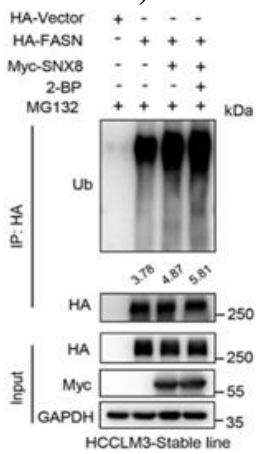

f)

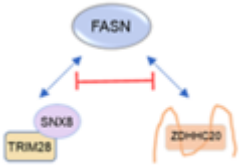

g)

Figure 6. ZDHHC20 promotes FASN protein stability by interfering with binding of the SNX8-TRIM28 complex to FASN

(a) Western blot analysis of Flag-tagged FASN levels in Huh7 cells transfected with Myc-tagged SNX8 in the presence or absence of HA-tagged ZDHHC20, (b) Western blot analysis of Flag-tagged FASN levels in Huh7 cells transfected with His-tagged TRIM28 in the presence or absence of HA-tagged ZDHHC20, (c) Co-IP evaluation of SNX8-FASN interaction in Huh7 cells with or without ZDHHC20 expression after MG132 (10 μM) treatment for 8 h, (d) Co-IP evaluation of TRIM28-FASN interaction in Huh7 cells with or without ZDHHC20 expression after MG132 (10 μM) treatment for 8 h, (e, f) Ubiquitination analysis of FASN in HCCLM3 cells stably expressing HA-vector or HA-tagged FASN following transfection with Flag-tagged TRIM28 (e) or Myc-tagged SNX8 (f), with or without 50 μM 2-BP for 24 h and subsequent MG132 (10 μM) for 8 h, and (g) Schematic representation of the mutually exclusive interactions between FASN-TRIM28-SNX8 and FASN-ZDHHC20.

Palmitoylation at cysteines 1471 and 1881 of FASN enhances its stability

The specific impact of palmitoylation at residues C1471 and C1881 was examined by expressing Flag-tagged C1471S, C1881S, and double C1471/1881S mutants in HCC cells. Cycloheximide chase assays showed accelerated degradation of the mutant proteins relative to wild-type FASN **(Figure 7a)**. These stability differences were corroborated by immunofluorescence, which demonstrated weaker fluorescence signals for the mutant variants **(Figure 7b)**. Ubiquitination levels were correspondingly higher in the mutants, most prominently in the double mutant **(Figure 7c)**.

Given ZDHHC20's role in promoting HCC and its control over FASN palmitoylation, the contribution of the ZDHHC20-FASN interaction to cellular behavior was evaluated. Proliferation assays (CCK-8 and colony formation) in cells expressing wild-type or mutant forms of FASN revealed significantly reduced growth upon mutation of the palmitoylation sites **(Figures 7d and 7e)**. In vivo studies using a cell-derived xenograft model similarly showed diminished tumor growth with mutant FASN compared with the wild-type version. Co-immunoprecipitation further indicated stronger binding of the palmitoylation-deficient mutants to TRIM28. These findings support the conclusion that ZDHHC20-mediated palmitoylation of FASN at C1471 and C1881 antagonizes ubiquitination by the SNX8-TRIM28 complex.

Analysis of clinical specimens from 10 HCC cases and matched adjacent normal tissues confirmed elevated protein expression of both ZDHHC20 and FASN in tumor samples compared with normal adjacent tissues.

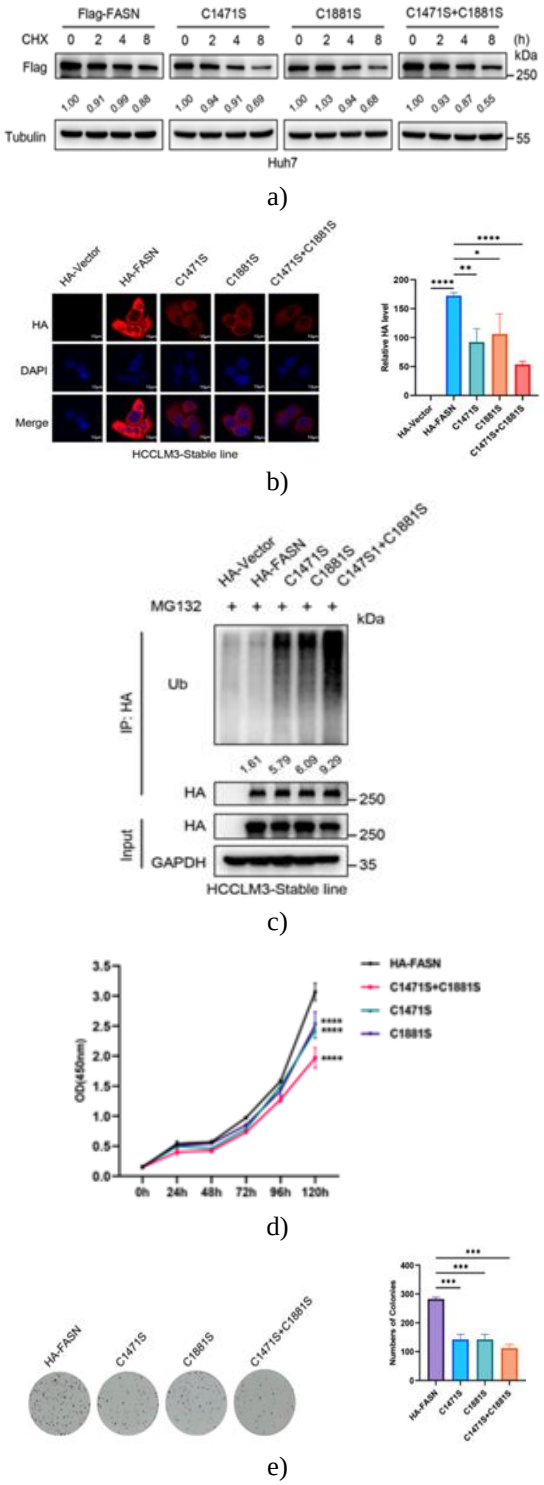

Figure 7. Impairment of palmitoylation at FASN cysteines 1471 and 1881 facilitates protein degradation

(a) FASN protein stability in Huh7 cells transfected with Flag-tagged wild-type FASN or the indicated cysteine-to-serine mutants following cycloheximide (CHX, 100 μg/ml) treatment, (b) Immunofluorescence staining for HA in HCCLM3 cells stably expressing HA-Vector, HA-tagged wild-type FASN, or the indicated mutants. DAPI indicates nuclei. Scale bar = 10 μm. (c) Ubiquitination levels of FASN in HCCLM3 cells stably expressing HA-Vector, HA-tagged wild-type FASN, or the indicated mutants after MG132 (10 μM) treatment for 8 h, and (d, e) Proliferation of HCCLM3 cells transduced with lentiviruses expressing HA-tagged wild-type FASN or the indicated mutants was assessed by CCK-8 assay (n = 3 biologically independent experiments, two-way ANOVA) (d) and colony formation assay (n = 3 biologically independent experiments, one-way ANOVA) (e).

Intracellular fatty acids serve as essential precursors for the synthesis of membrane lipids, signaling molecules, and various modifications [29, 30]. They also provide an alternative energy supply that supports tumor expansion. Although substantial progress has been achieved in elucidating the role of palmitoylation in fatty acid-related disorders, the precise mechanisms through which this modification drives hepatocarcinogenesis remain incompletely understood. The present study establishes that ZDHHC20-dependent palmitoylation of FASN prevents its ubiquitination. Consequently, genetic deletion of ZDHHC20 leads to decreased lipid synthesis and attenuated liver cancer progression both in vitro and in vivo **(Figure 8)**. These results uncover a previously unrecognized pathway involving ZDHHC20 that is central to HCC development.

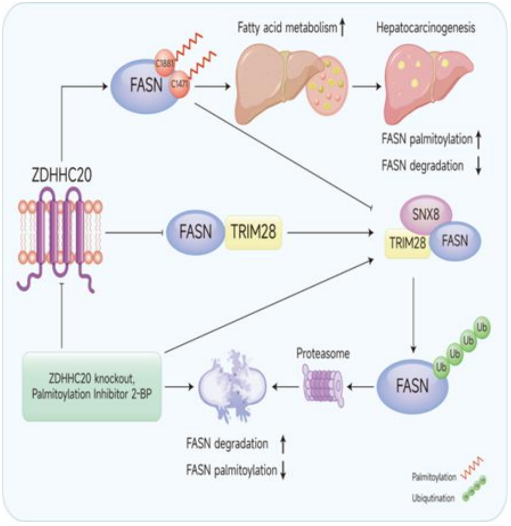

Figure 8. Schematic representation summarizing the overall experimental design and molecular mechanism elucidated in this study.

Mechanistically, palmitoylation of FASN at cysteines 1471 and 1881 by ZDHHC20 interferes with its recruitment to the SNX8-TRIM28 complex. This competitive interplay is essential for maintaining FASN stability during HCC development. Suppression of FASN palmitoylation strengthens its association with the SNX8-TRIM28 complex, providing new insight into how palmitoylation controls FASN abundance. The identification of novel regulators of FASN expression may uncover additional mechanisms underlying disease pathogenesis. Moreover, clarifying the dynamic equilibrium between ZDHHC20-mediated FASN palmitoylation and SNX8-TRIM28 binding could inform the design of therapeutic strategies to interrupt oncogenic cascades in HCC and enhance clinical outcomes.

FASN participates in the S-palmitoylation of several important proteins, including GSDMD in macrophages, endothelial nitric-oxide synthase (eNOS) in endothelial cells, and MYD88 in neutrophils [51, 52]. As the enzyme responsible for generating palmitate, FASN is indispensable for protein palmitoylation. Accumulating evidence indicates that FASN-substrate interactions are necessary for effective palmitoylation. The current work demonstrates that FASN itself undergoes palmitoylation; however, it remains uncertain whether FASN must be palmitoylated to facilitate the modification of other target proteins.

Proteomic profiling of palmitoylated proteins in this study identified multiple candidates whose modification was diminished upon ZDHHC20 knockout. Potential substrates and specific palmitoylation sites for ZDHHC20 were uncovered, with two sites on FASN (C1471 and C1881) rigorously validated through multiple experimental approaches. Nevertheless, the relative importance of each site for HCC progression has not been determined. Additional studies are required to clarify whether ZDHHC20 modifies both residues simultaneously or sequentially.

Recent reports indicate elevated ZDHHC20 expression in breast, lung, and pancreatic cancers, suggesting that its inhibition may hold therapeutic promise [25, 53, 54]. Beyond oncology, emerging evidence reveals broader functions of ZDHHC20 in immunity, inflammation, viral infection, and cellular regulation. For instance, Chopard *et al*. [55] showed that ZDHHC20 palmitoylates HIV-Tat, thereby enhancing its affinity for PI(4,5)P2 in uninfected cells. Another study linked ZDHHC20-regulated palmitoylation of the Spike protein to its fusogenic activity and facilitation of SARS-CoV-2 entry [56]. ZDHHC20 has also been shown to palmitoylate IFITM3, contributing to antiviral defense [57]. Furthermore, Lu *et al*. [58] identified ZDHHC20-mediated S-palmitoylation of CD80 as a regulatory mechanism in T cell activation. Notably, Bu *et al*. [59] reported that PA-ZDHHC17/24-mediated palmitoylation of AKT activates AKT independently of PIP3, promoting NASH and liver tumorigenesis. This work suggests potential HCC treatment strategies involving PA-restricted diets, inhibition of palmitate synthesis, or direct targeting of AKT palmitoylation [59]. Structural and mechanistic insights from these studies have advanced our understanding of how ZDHHC20 selects and modifies its substrates. The diverse cellular effects of palmitoylation likely arise from context-dependent substrate preferences of palmitoyltransferases across different tissues. The present data confirm the tumor-promoting activity of ZDHHC20 in HCC and its positive regulation of fatty acid metabolism, positioning the ZDHHC20-FASN axis as a promising anti-cancer target. Overall, these findings highlight ZDHHC20's role in hepatocarcinogenesis by stabilizing FASN and suggest its potential as a therapeutic target in HCC.

Conclusion

In summary, this study demonstrates that ZDHHC20 promotes hepatocarcinogenesis and establishes FASN as a ZDHHC20 substrate, palmitoylated at cysteines 1471 and 1881. Moreover, ZDHHC20-mediated FASN palmitoylation antagonizes degradation through the ubiquitin-proteasome pathway involving the E3 ligase complex SNX8-TRIM28. These insights advance our understanding of HCC pathogenesis and identify potential targets for precision molecular therapy.

Acknowledgments: None

Conflict of Interest: None

Financial Support: None

Ethics Statement: None

References

1. Schmidt MF, Schlesinger MJ. Fatty acid binding to vesicular stomatitis virus glycoprotein: a new type of

post-translational modification of the viral glycoprotein. Cell. 1979;17(4):813-9.
2. Linder ME, Deschenes RJ. Palmitoylation: policing protein stability and traffic. Nat Rev Mol Cell Biol. 2007;8(1):74-84.
3. Roth AF, Feng Y, Chen L, Davis NG. The yeast DHHC cysteine-rich domain protein Akr1p is a palmitoyl transferase. J Cell Biol. 2002;159(1):23-8.
4. Runkle KB, Kharbanda A, Stypulkowski E, Cao XJ, Wang W, Garcia BA, et al. Inhibition of DHHC20-Mediated EGFR Palmitoylation creates a dependence on EGFR Signaling. Mol Cell. 2016;62(3):385-96.
5. Le X, Huang Y, Li Y, Wang X, Zhang Q, Liu Z, et al. DNA methylation downregulated ZDHHC1 suppresses tumor growth by altering cellular metabolism and inducing oxidative/ER stress-mediated apoptosis and pyroptosis. Theranostics. 2020;10(21):9495-511.
6. Zhang Z, Li X, Yang F, Chen C, Liu P, Ren Y, et al. DHHC9-mediated GLUT1 S-palmitoylation promotes glioblastoma glycolysis and tumorigenesis. Nat Commun. 2021;12(1):5872.
7. Chen S, Zhu B, Yin C, Liu W, Han C, Chen B, et al. Palmitoylation-dependent activation of MC1R prevents melanomagenesis. Nature. 2017;549(7672):399-403.
8. Fraser NJ, Howie J, Wypijewski KJ, Fuller W. Therapeutic targeting of protein S-acylation for the treatment of disease. Biochem Soc Trans. 2020;48(1):281-90.
9. Ponimaskin E, Dityatev A, Ruonala MO, Fukata M, Fukata Y, Kobe F, et al. Fibroblast growth factor-regulated palmitoylation of the neural cell adhesion molecule determines neuronal morphogenesis. J Neurosci. 2008;28(36):8897-907.
10. Liao D, Li Y, Yang J, Wang H, Chen X, Liu T. The role of s-palmitoylation in neurological diseases: implication for zDHHC family. Front Pharmacol. 2023;14:1342830.
11. Ko PJ, Dixon SJ. Protein palmitoylation and cancer. EMBO Rep. 2018;19(10).
12. Liu Z, Xiao M, Mo H, Wang H, Li Y, Zhao Q, et al. Emerging roles of protein palmitoylation and its modifying enzymes in cancer cell signal transduction and cancer therapy. Int J Biol Sci. 2022;18(8):3447-57.
13. Marino M, Ascenzi P. Membrane association of estrogen receptor alpha and beta influences 17beta-estradiol-mediated cancer cell proliferation. Steroids. 2008;73(9-10):853-8.
14. Pedram A, Razandi M, Deschenes RJ, Levin ER. DHHC-7 and -21 are palmitoylacyltransferases for sex steroid receptors. Mol Biol Cell. 2012;23(1):188-99.
15. Chen X, Ma H, Wang Z, Zhang S, Yang H, Qin Z, et al. DHHC protein family targets different subsets of glioma stem cells in specific niches. J Exp Clin Cancer Res. 2019;38(1):25.
16. Chen X, Ma H, Wang Z, Zhang S, Yang H, Qin Z, et al. EZH2 palmitoylation mediated by ZDHHC5 in p53-Mutant glioma drives Malignant Development and Progression. Cancer Res. 2017;77(18):4998-5010.
17. Siegel RL, Giaquinto AN, Jemal A. Cancer statistics, 2024. CA Cancer J Clin. 2024;74(1):12-49.
18. Vogel A, Meyer T, Sapisochn G, Salem R, Saborowski A. Hepatocellular carcinoma. Lancet. 2022;400(10360):1345-62.
19. Villanueva A. Hepatocellular Carcinoma. N Engl J Med. 2019;380(15):1450-62.
20. Brown ZJ, Tsilimigras DI, Ruff SM, Mohseni A, Kamel IR, Cloyd JM, et al. Management of Hepatocellular Carcinoma: a review. JAMA Surg. 2023;158(4):410-20.
21. Yamada K, Uchiyama K, Kitazawa T, Hara T, Saito T, Yamada M, et al. Unconventional secretion of PKCdelta exerts tumorigenic function via stimulation of ERK1/2 signaling in Liver Cancer. Cancer Res. 2021;81(2):414-25.
22. Rana MS, Kumar P, Lee CJ, Verardi R, Rajashankar KR, Banerjee A. Fatty acyl recognition and transfer by an integral membrane S-acyltransferase. Science. 2018;359(6372).
23. Kharbanda A, Runkle K, Stypulkowski E, Wang W, Wei Z, Zhang X, et al. Blocking EGFR palmitoylation suppresses PI3K signaling and mutant KRAS lung tumorigenesis. Sci Signal. 2020;13(621).
24. Wang W, Runkle KB, Terrones O, Wang Y, Karginov TA, Hannoush RN. Protein depalmitoylation is induced by Wnt5a and promotes polarized cell behavior. J Biol Chem. 2015;290(25):15707-16.
25. Tomic G, Bhopalwala H, Baysal M, Khan A, Zhang J, Singh G, et al. Palmitoyl transferase ZDHHC20 promotes pancreatic cancer metastasis. Cell Rep. 2024;43(5):114224.

26. Ocasio CA, Baggelaar MP, Sipthorp J, Tomkinson NC, Tate EW. A palmitoyl transferase chemical-genetic system to map ZDHHC-specific S-acylation. Nat Biotechnol. 2024;42(10):1548-58.
27. Feng R, Li S, Wang Y, Zhang Q, Chen H, Liu Z, et al. Identification and validation of palmitoylation metabolism-related signature for liver hepatocellular carcinoma. Biochem Biophys Res Commun. 2024;692:149325.
28. Altenberg B, Greulich KO. Genes of glycolysis are ubiquitously overexpressed in 24 cancer classes. Genomics. 2004;84(6):1014-20.
29. Zaidi N, Lupien L, Kuemmerle NB, Kinlaw WB, Swinnen JV, Smans K. Lipogenesis and lipolysis: the pathways exploited by the cancer cells to acquire fatty acids. Prog Lipid Res. 2013;52(4):585-9.
30. Bian X, Liu R, Meng Y, Xing D, Xu D, Lu Z. Lipid metabolism and cancer. J Exp Med. 2021;218(1).
31. Jiang L, Wang X, Zhang J, Li Y, Zhao J, Liu Y, et al. Up-regulated FASN expression promotes transcoelomic metastasis of ovarian cancer cell through epithelial-mesenchymal transition. Int J Mol Sci. 2014;15(7):11539-54.
32. Chianese U, Papulino C, De Micco M, Nocentini A, Supuran CT, Altucci L, et al. FASN multi-omic characterization reveals metabolic heterogeneity in pancreatic and prostate adenocarcinoma. J Transl Med. 2023;21(1):32.
33. Bruning U, Morales-Rodriguez F, Kalucka J, Goveia J, Taverna F, Queiroz KC, et al. Impairment of angiogenesis by fatty acid synthase inhibition involves mTOR malonylation. Cell Metab. 2018;28(6):866-e88015.
34. Zaytseva YY, Rychahou PG, Gulhati P, Elliott VA, Mustain WC, O'Connor K, et al. Cancer cell-associated fatty acid synthase activates endothelial cells and promotes angiogenesis in colorectal cancer. Carcinogenesis. 2014;35(6):1341-51.
35. Sun Y, Wang Q, Liu H, Li X, Zhang Y, Chen Z, et al. Apoptosis induction in human prostate cancer cells related to the fatty acid metabolism by wogonin-mediated regulation of the AKT-SREBP1-FASN signaling network. Food Chem Toxicol. 2022;169:113450.
36. Menendez JA, Lupu R. Fatty acid synthase and the lipogenic phenotype in cancer pathogenesis. Nat Rev Cancer. 2007;7(10):763-77.
37. Fhu CW, Ali A. Fatty acid synthase: an emerging target in Cancer. Molecules. 2020;25(17).
38. Xiao Y, Li S, Chen Y, Zhang L, Wang H, Yang J, et al. The implications of FASN in immune cell biology and related diseases. Cell Death Dis. 2024;15(1):88.
39. Buckley D, Duke G, Heuer TS, O'Farrell M, Wagman AS, McCulloch W, et al. Fatty acid synthase - modern tumor cell biology insights into a classical oncology target. Pharmacol Ther. 2017;177:23-31.
40. Xu S, Zhang Y, Liu X, Wang J, Li M, Zhao L, et al. TRIM56 protects against nonalcoholic fatty liver disease by promoting the degradation of fatty acid synthase. J Clin Invest. 2024;134(5).
41. Zeng H, Qin H, Liao M, Zheng E, Feng X, Lin X, et al. CD36 promotes de novo lipogenesis in hepatocytes through INSIG2-dependent SREBP1 processing. Mol Metab. 2022;57:101428.
42. Li L, Pilo GM, Li X, Cigliano A, Latte G, Che L, et al. Inactivation of fatty acid synthase impairs hepatocarcinogenesis driven by AKT in mice and humans. J Hepatol. 2016;64(2):333-41.
43. Hu J, Che L, Li L, Pilo GM, Cigliano A, Ribback S, et al. Co-activation of AKT and c-Met triggers rapid hepatocellular carcinoma development via the mTORC1/FASN pathway in mice. Sci Rep. 2016;6:20484.
44. Nelson ME, Lahiri S, Chow JD, Byrne FL, Hargett SR, Breen DS, et al. Inhibition of hepatic lipogenesis enhances liver tumorigenesis by increasing antioxidant defence and promoting cell survival. Nat Commun. 2017;8:14689.
45. Hu Y, Wang R, Zhang Y, Huang Y, Liu C, Li X, et al. Fatty acid synthase-suppressor screening identifies sorting Nexin 8 as a therapeutic target for NAFLD. Hepatology. 2021;74(5):2508-25.
46. Li N, Zhou ZS, Shen Y, Xu J, Miao HH, Xiong Y, et al. Inhibition of the sterol regulatory element-binding protein pathway suppresses hepatocellular carcinoma by repressing inflammation in mice. Hepatology. 2017;65(6):1936-47.
47. Li XQ, Zhang Y, Wang L, Chen J, Liu H, Zhao Y, et al. beta-arrestin2 regulating beta2-adrenergic receptor signaling in hepatic stellate cells contributes to hepatocellular carcinoma progression. J Cancer. 2021;12(24):7287-99.
48. Li Z, Chen Y, Zhang X, Wang Y, Liu Q, Zhao J, et al. microRNA-199a-3p inhibits hepatic apoptosis and hepatocarcinogenesis by targeting PDCD4. Oncogenesis. 2020;9(10):95.

49. Kuhajda FP. Fatty-acid synthase and human cancer: new perspectives on its role in tumor biology. Nutrition. 2000;16(3):202-8.
50. Brigidi GS, Bamji SX. Detection of protein palmitoylation in cultured hippocampal neurons by immunoprecipitation and acyl-biotin exchange (ABE). J Vis Exp. 2013;(72).
51. Kim YC, Lee SE, Kim SK, Jang HD, Hwang I, Kim JH, et al. Toll-like receptor mediated inflammation requires FASN-dependent MYD88 palmitoylation. Nat Chem Biol. 2019;15(9):907-16.
52. Wei X, Schneider JG, Shenouda SM, Lee A, Towler DA, Chakravarthy MV, et al. De novo lipogenesis maintains vascular homeostasis through endothelial nitric-oxide synthase (eNOS) palmitoylation. J Biol Chem. 2011;286(4):2933-45.
53. Draper JM, Smith CD. DHHC20: a human palmitoyl acyltransferase that causes cellular transformation. Mol Membr Biol. 2010;27(2-3):123-36.
54. Korycka J, Kłyszejko AL, Kojro E, Król M, Biernatowska A, Sikorski AF, et al. Human DHHC proteins: a spotlight on the hidden player of palmitoylation. Eur J Cell Biol. 2012;91(2):107-17.
55. Chopard C, Marquet R, Basyuk E, Roux P, Bertrand E, Bénichou S, et al. Cyclophilin A enables specific HIV-1 Tat palmitoylation and accumulation in uninfected cells. Nat Commun. 2018;9(1):2251.
56. Mesquita FS, Abrami L, Linder ME, van der Goot FG. SARS-CoV-2 hijacks a cell damage response, which induces transcription of a more efficient Spike S-acyltransferase. Nat Commun. 2023;14(1):7302.
57. McMichael TM, Zhang L, Chemudupati M, Hach JC, Kenney AD, Hang HC, et al. The palmitoyltransferase ZDHHC20 enhances interferon-induced transmembrane protein 3 (IFITM3) palmitoylation and antiviral activity. J Biol Chem. 2017;292(52):21517-26.
58. Lu B, Wang X, Chen S, Li Y, Zhang Z, Liu H, et al. zDHHC20-driven S-palmitoylation of CD80 is required for its costimulatory function. Acta Pharmacol Sin. 2024;45(6):1214-23.
59. Bu L, Zhang Y, Wang H, Li Q, Chen X, Liu Y, et al. High-fat diet promotes liver tumorigenesis via palmitoylation and activation of AKT. Gut. 2024;73(7):1156-68.